

RESEARCH LETTER

Open Access



Numerical simulation of a heavy rainfall event over Mindanao, Philippines, on 03 May 2017: mesoscale convective systems under weak large-scale forcing

Cathrene Lagare^{1*} , Takeshi Yamazaki¹ and Junshi Ito¹

Abstract

A heavy rainfall event caused by mesoscale convective systems (MCSs) resulted in flooding over areas of Davao City in Mindanao Island, Philippines, on 03 May 2017. The event occurred during the summer season (April–May) under weak large-scale conditions. This study investigated the initiation and development of MCSs by performing high-resolution numerical simulations with the finest grid spacing of 200 m, using the Weather Research and Forecasting (WRF) model. It was found that the merging of two meso- β scale convective systems over the west and east of Mount Apo caused the flood-producing rainfall in the Davao area. Results show that the west meso- β scale convective system formed over the basin area in Mindanao Island due to moisture advection from sea breeze circulation. In addition, the concave geometry of the Mindanao basin assisted in accumulating moisture which made the basin favorable for convection development. Meanwhile, the precipitating downdrafts generated cold pools wherein the continuous convergence of multiple outflow boundaries resulted in the further development and maintenance of the MCS over the basin. While the east meso- β scale convective system developed over the Davao area due to the interaction between southeasterlies (ambient trade winds) and Mount Apo terrain. Merging of the MCSs resulted in the development of a larger meso- β scale system. Eventually, the larger meso- β scale convective system split and splitted MCSs weakened over time.

Keywords MCS, Heavy rainfall, Cold pool, The Philippines

Introduction

Long-lived mesoscale convective systems (MCSs) may cause heavy to extreme rainfall that can lead to large economic and human damages. MCS arises from convection initiation and upscale growth of the system (Du et al. 2020). For an MCS to develop, abundant moisture, lifting mechanism, instability, and vertical wind shear are essential (Wang et al. 2013; Schumacher and Rasmussen 2020).

Multiple observational (Kawashima et al. 2011; Keenan et al. 2000; Kuo and Chen 1990) and numerical (Du et al. 2020; Yulihastin et al. 2022; Zhang et al. 2003; Miao and Yang 2020) studies have already been conducted over the western North Pacific and Maritime Continent to investigate the processes related to the initiation and development of convective storms. Convections in the Maritime Continent are strongly influenced by coastal and diurnal effects (Yang and Slingo 2001; Yulihastin et al. 2022). Mori et al. (2004) found that convections over Sumatra Island, Indonesia are initiated by local convergence of sea breeze encountering the mountain range along the coastline and land breeze converging with the background wind flow. Qian (2008) also identified similar convection

*Correspondence:

Cathrene Lagare
clagare@dc.tohoku.ac.jp

¹ Graduate School of Science, Tohoku University, Sendai, Japan



© The Author(s) 2023, corrected publication 2023. **Open Access** This article is licensed under a Creative Commons Attribution 4.0 International License, which permits use, sharing, adaptation, distribution and reproduction in any medium or format, as long as you give appropriate credit to the original author(s) and the source, provide a link to the Creative Commons licence, and indicate if changes were made. The images or other third party material in this article are included in the article's Creative Commons licence, unless indicated otherwise in a credit line to the material. If material is not included in the article's Creative Commons licence and your intended use is not permitted by statutory regulation or exceeds the permitted use, you will need to obtain permission directly from the copyright holder. To view a copy of this licence, visit <http://creativecommons.org/licenses/by/4.0/>.

development mechanisms over Java Island, Indonesia, and are mainly associated with sea breeze convergence over the island, enhanced by mountain–plain winds, and further intensified by cumulus merger processes.

Meanwhile, over the Philippines, Natoli and Maloney (2019) studied the relationship between the diurnal cycle of precipitation and the Boreal Summer Intraseasonal Oscillation (BSISO). Results showed that during boreal summer (May–October), the precipitation diurnal cycle peaks over land from late afternoon to early evening and propagates westward towards the South China Sea. Bañares et al. (2021) also examined the seasonal and diurnal characteristics of localized convective rainfall events in Metro Manila, Philippines, using weather station observations from 2013 to 2014. Results show that high rainfall amounts were observed over the northern and central areas of Metro Manila as compared with the southern area during the northeast monsoon season (November–March), summer season (April–May), and southwest monsoon season (June–October). During the summer season, wherein tropical cyclones (TCs) and monsoonal influences are absent, convective rainfall events tend to occur in the afternoon.

Mindanao Island in the southern part of the Philippines frequently experiences heavy rainfall, and studies have shown its interaction with strong synoptic-scale systems (Faustino-Eslava et al. 2011; Olaguera et al. 2021; Yumul et al. 2013). However, during the summer season, where apparent large-scale systems are absent, the fraction of MCS rainfall to the total rainfall still reaches 30–65%, suggesting that localized convective systems largely contribute to the rainfall in Mindanao Island (refer to Additional file 1: Fig. S1). Understanding the initiation and development of localized heavy rainfall under weak large-scale forcings using numerical simulations have recently been examined in Oahu, Hawaii (Hsiao et al. 2020) and south of Beijing, China (Xiao et al. 2022), for example. However, to the best of the authors' knowledge, there is no literature yet on numerical studies on MCSs related to localized convection over Mindanao Island, Philippines.

The present work investigates the local convective processes over Mindanao Island by employing numerical simulations on an event under a condition where large-scale systems have seemingly little influence on convection development. On 03 May 2017, a severe rainfall event over Davao City in Mindanao Island, Philippines, resulted in flooding in the urban area. A previous hydrological study has investigated the flood during this event (Macalalad et al. 2021). Still, a better understanding of

the physical processes related to the development of the convective systems that caused the flood is needed to improve the prediction of these hazardous systems. This is the first attempt to use numerical simulations on MCSs over Mindanao Island.

Case overview

Figure 1a shows the synoptic environment over the Philippines on 03 May 2017. No frontal system was present near Mindanao Island. The vertically integrated moisture flux from the surface to 100 hPa was also calculated using the European Center for Medium-Range Weather Forecasts (ECMWF) ERA5 (Hersbach et al. 2020) reanalysis to examine the moisture coming from large-scale systems and is given by

$$\langle q\mathbf{v} \rangle = \frac{1}{g} \int_{100\text{hPa}}^{p_{\text{surface}}} q\mathbf{v} dp, \quad (1)$$

where q is specific humidity, \mathbf{v} is wind vector, p is pressure, and g is the gravitational acceleration. As shown in Fig. 1b, easterlies were the prevailing winds, with weak wind conditions ($<5.5 \text{ m s}^{-1}$) during the summer season. High moisture fluxes were present over the northern Philippines due to the frontal systems, but these were far from Mindanao Island. This implies that only a little moisture from large-scale systems was directly transported to Mindanao Island. The absence of apparent synoptic forcing suggests that the rainfall event over Mindanao Island was due to localized processes.

Figure 2 shows the hourly evolution of the convection distribution observed over parts of Mindanao Island on 03 May 2017 from the temperature black body (TBB) of the Himawari-8 satellite. At 11:00 LST, there were no convections yet over the basin area of Mindanao Island (see Fig. 1c). As it reached 12:00 LST, convections were observed over the basin, which developed into a meso- β scale convective system¹ at 14:00 LST and weakened over time. Meanwhile, two more meso- β scale convective systems developed around the Mount Apo terrain (see Fig. 1c) at 19:00 LST, referred to as MCS-1 and MCS-2 in Fig. 2i. A weather station in Davao City (Matina Station of the Manila Observatory; refer to Fig. 1c) measured a 62.25 mm h^{-1} rainfall in the evening (20:00 LST) as MCS-1 and MCS-2 organized into a single larger meso- β scale convective system (referred to as MCS-3 in Fig. 2j) resulting in the heavy rainfall that caused the flooding in Davao City at night. Afterwards, MCS-3 weakened and dissipated. The target MCSs of this study are these MCSs.

¹ The mesoscale definition is based on the scaling method of Orlanski (1975).

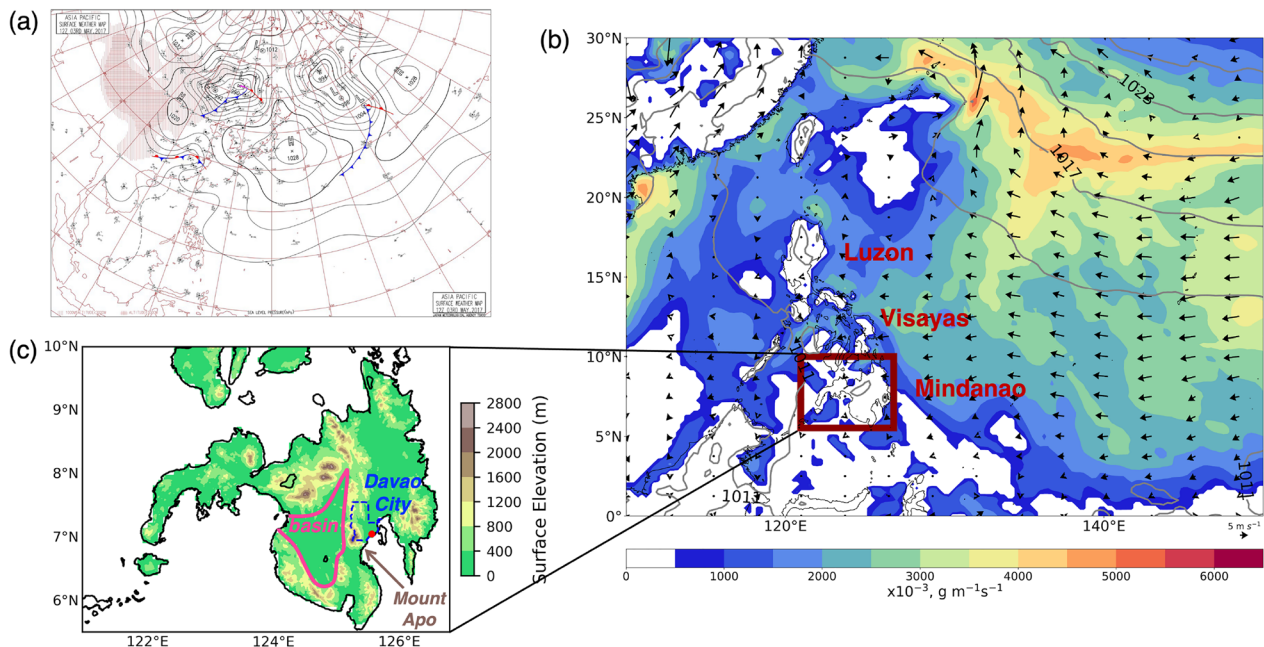


Fig. 1 Synoptic conditions on 03 May 2017 based on **a** the Asia Pacific surface analysis map from Japan Meteorological Agency and **b** vertically integrated moisture flux from surface to 100 hPa (shade), mean sea level pressure (grey contour), and 850 hPa wind vectors from ERA5 reanalysis at 20:00 LST. The three major islands of the Philippines (Luzon, Visayas, and Mindanao) are labeled in **(b)**, and the surface elevation map of Mindanao Island where the basin (solid pink line), Davao City (broken blue line), Mount Apo, and location of the Matina Weather Station (red dot) are demarcated in **c**

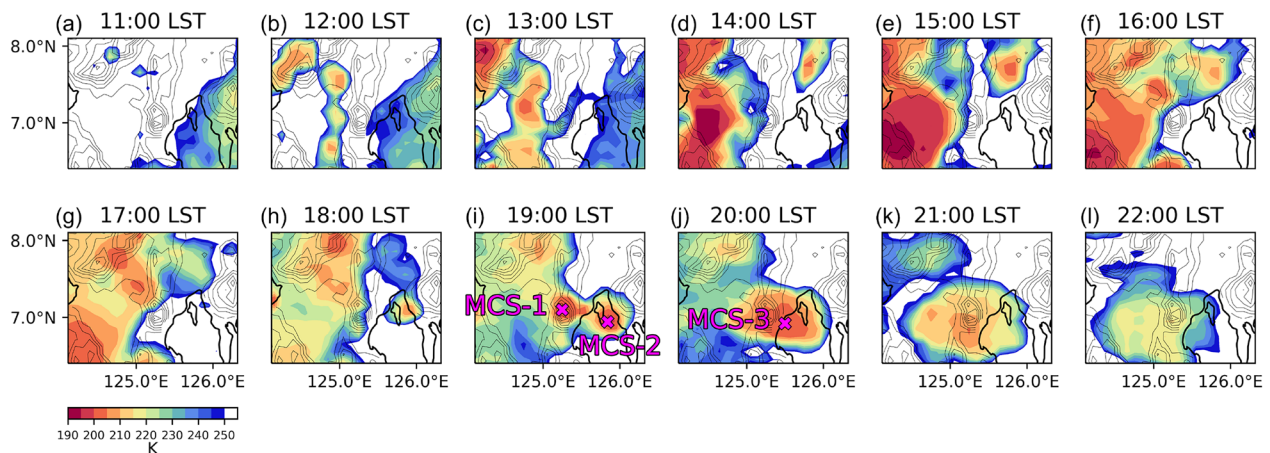


Fig. 2 a-l Hourly evolution of convection distribution from TBB of Himawari-8 Satellite with topography (contour with intervals of 400 m) over parts of Mindanao Island. The “X” markers in **i, j** denote the locations of MCS-1, MCS-2, and MCS-3

Numerical simulations

In this study, the MCSs were simulated using the Advanced Research Weather Research and Forecasting (WRF-ARW; Skamarock et al. 2019) model version 4.2.2. The simulations were run from 19:00 UTC 02 to 0:00 UTC 04 May 2017 at 60 vertical levels. As shown in Fig. 3, five nested domains were used. Two-way nesting

was applied to horizontal resolutions dx of 27, 9, 3, and 1 km, while one-way nesting to $dx = 200$ m. The initial and boundary conditions of the parent domain were from the hourly ERA5 reanalysis data at 0.25 degree resolution. The physics parameterization schemes used in the model include the Kain–Fritsch (Kain 2004) cumulus scheme, WRF Single–Moment 6–Class (WSM6;

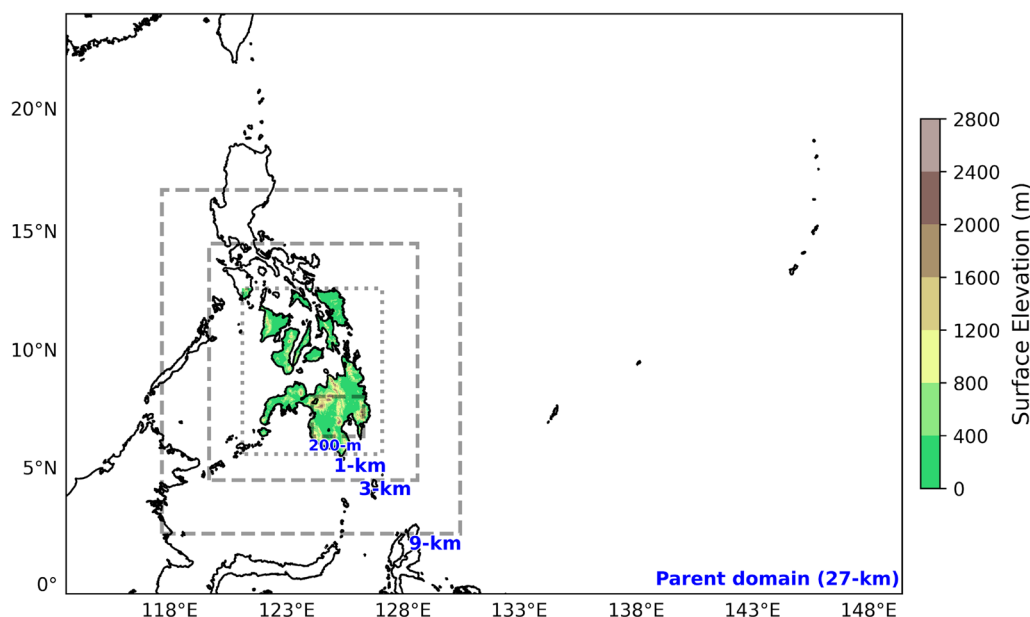


Fig. 3 Model domains with surface elevation (m)

Hong and Lim 2006) microphysics scheme, and Asymmetric Convection Model 2 (ACM2; Pleim 2007) planetary boundary layer (PBL) scheme, Dudhia (Dudhia 1989) shortwave scheme, and Rapid Radiative Transfer Model (RRTM; Mlawer et al. 1997) longwave radiation scheme. The parameterization schemes and calibrated values for the Kain–Fritsch cumulus scheme of Tolentino and Bagtasa (2021) were followed. The model configuration is summarized in Additional file 1: Table S1. Note that the cumulus scheme was turned off for $dx = 3$ km, 1 km, and 200 m, assuming the grid spacings were fine enough to resolve convection. Meanwhile, the innermost domain ($dx = 200$ m) was run on a large-eddy simulation (LES) mode where the PBL was turned off, and three-dimensional turbulence diffusion was turned on.

Results and discussion

Model evaluation

Figure 4 shows the hourly evolution of the derived reflectivity from $dx = 200$ m and was compared with the Himawari-8 satellite observation (Fig. 2) to evaluate the model performance. The model reasonably reproduced the convections over the basin area from 11:00 LST and captured MCS-1 and MCS-2 at 19:00 LST, and MCS-3 at 20:00 LST.

The model outputs at different horizontal resolutions were compared with the observation data. Rainfall data from 53 automated weather stations of the Department of Science and Technology-Advanced Science and

Technology Institute (DOST-ASTI), Philippines, were used as observation in Fig. 5.

Figure 5a–f shows the spatial distribution of the 9 h of accumulated rainfall (from 14:00 LST to 23:00 LST of 03 May 2017) of observation and model. The model was able to generally simulate the spatial distribution and peaks of the localized rainfall across resolutions. Increasing dx from 27 km to finer resolutions resulted in simulating higher rainfall intensities and sharper spatial patterns.

The hourly mean rainfall is also shown in Fig. 5g and is calculated by area-averaging the rainfall values based on the observation points demarcated in Fig. 5a. The hourly model rainfall across various resolutions generally shows good correspondence with the observation. However, there is 3-h delay for the largest rainfall peaks of the models. Meanwhile, downscaling the model to $dx = 200$ m produced an overestimated peak. Nevertheless, $dx = 200$ m resulted in better performance, as demonstrated by evaluating the threat scores of the 9 h of accumulated rainfall (similar timesteps to Fig. 5a–f) at a given threshold, as shown in Fig. 5h. The results clearly show that the threat scores of $dx = 200$ m at thresholds above 25 mm prevail over those of coarser resolutions, which reveals the improved reproducibility of heavy rainfall.

Regardless of the differences between the model and observation, there is still a generally good agreement which made it reasonable to use the model results in the analyses of the convection development. Specifically, $dx = 200$ m results are used in “Convection development” and “Merging and splitting of MCSs” sections.

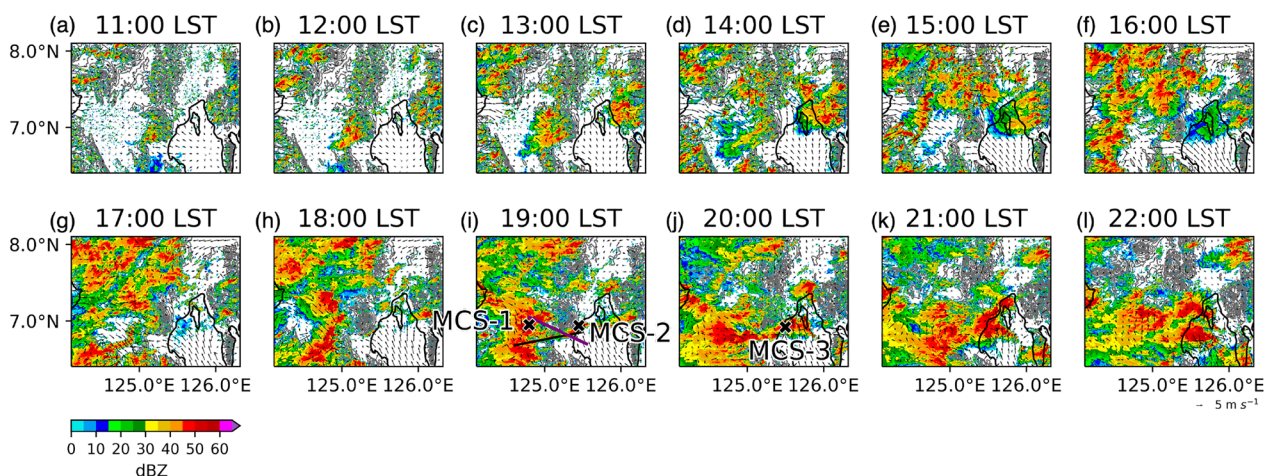


Fig. 4 a-l Hourly evolution of the simulated radar reflectivities (the maximum in a vertical column at each horizontal position) of $dx = 200$ m with topography (contour with intervals of 400 m) over parts of Mindanao Island. The black and purple transects in **i** represent the cross-sections used in Fig. 8. The "X" markers in **i, j** denote the locations of MCS-1, MCS-2, and MCS-3

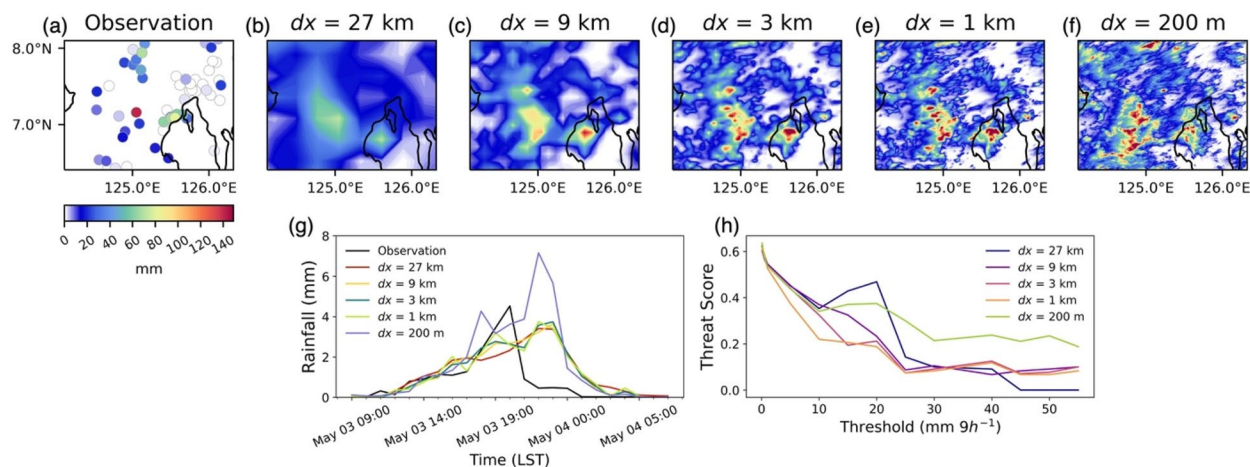


Fig. 5 Spatial distributions of 9 h of accumulated **a** observation and **b-f** model rainfall (14:00–23:00 LST of 03 May 2017) at different horizontal resolutions, and **g** area-averaged hourly mean rainfall over the area in **a**; **h** threat scores at different threshold values of the 9 h of accumulated rainfall in **a-f**

Convection development

Simulations show that MCSs indeed caused the heavy rainfall in Mindanao Island. Two prominent meso- β scale convective systems are found to develop west and east of the Mount Apo terrain in Mindanao Island (MCS-1 and MCS-2, respectively). This section aims to identify the processes that influenced the formation and development of these MCSs.

Development of MCS-1 (west of Mount Apo)

Figure 6a–d shows the evolution of the vertically integrated moisture fluxes (from the surface to 900 hPa) of $dx = 200$ m. The results show that the concave basin played an important role in accumulating the moisture

brought from the ocean towards the inland. In fact, from 11:00 LST to 17:00 LST, moisture has been gradually transported to the basin. At 17:00 LST, the presence of abundant moisture within the basin made it conducive for convection development as the concave geometry of the terrain promoted inland low-level moistening (Du et al. 2020). The instability in the basin is also demonstrated by the large increase of maximum convective available potential energy (MCAPE) from 1661.6 J kg⁻¹ at 11:00 LST to 2284.0 J kg⁻¹ at 14:00 LST (area-averaged over the black-boxed area in Fig. 6c). Figure 6e shows the Hovmöller diagram of 10 m zonal winds (shade) and 950 hPa specific humidity (contour), area-averaged over the black-boxed region in Fig. 6c. It demonstrates that the

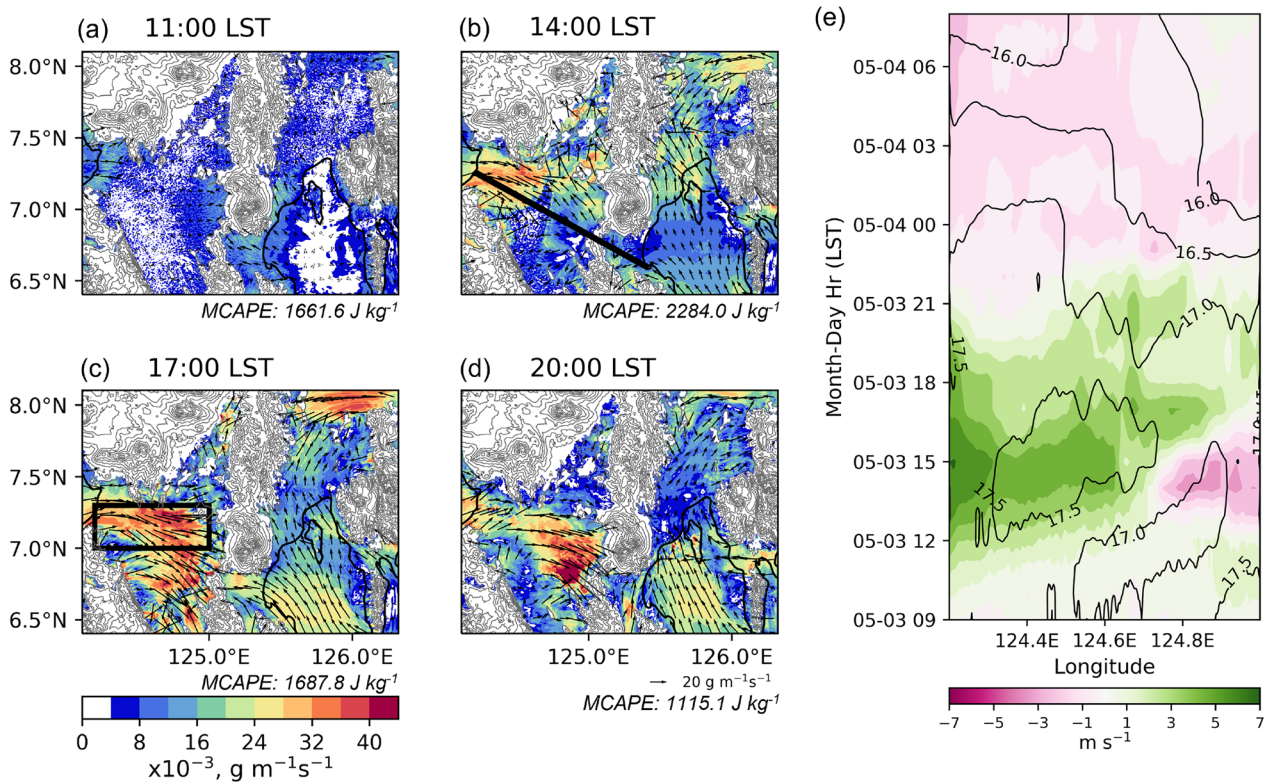


Fig. 6 a–d Vertically integrated moisture flux with vectors (from surface to 900 hPa) and topography for a 11:00 LST, b 14:00 LST, c 17:00 LST, and d 20:00 LST. e Hovmöller diagram of 10 m zonal winds (shade) with specific humidity at 950 hPa (contour) area-averaged over the black-boxed area in c. $dx = 200$ m results are used. The black transect in b represents the cross-section used in Additional file 1: Figs. S2 and S3. The values on the lower right of a–d represent their corresponding MCAPE value. MCAPE values are area-averaged over the black-boxed area in c

moisture movement from the ocean to inland was due to sea breeze circulation. The sea breeze circulation gradually started at 10:00 LST and was strongest at around 13:00 LST to 17:00 LST, followed by an increase in the low-level specific humidity over the basin. The convection due to sea breeze circulation is further supported by the cross-section of winds (black transect in Fig. 6b) shown in Additional file 1: Fig. S2. As the strong winds from the northwest coastline reached the center of the basin, the convergence with the opposing southeasterly winds triggered convection.

As shown in Fig. 4e–g, convections formed over the foot of the mountains and the center of the basin triggered by sea breeze circulations. The convections that developed over the center of the basin generated cold pools due to evaporative cooling of the precipitating downdrafts (Fig. 7): to investigate the formation of cold pools, we use the isentropic analysis method of Iwasaki et al. (2014), where a cold air mass is defined as an air mass below a threshold potential temperature. Cold air mass amount (DP), which is the pressure difference between the ground and θ_T surface, and DP flux (\overline{MF}) are calculated as follows:

$$DP \equiv p_s - p(\theta_T), \quad (2)$$

$$\overline{MF} \equiv \int_{p(\theta_T)}^{p_s} \mathbf{v} dp, \quad (3)$$

where θ is potential temperature, p_s is surface pressure, $p(\theta_T)$ is pressure on isentropes $\theta = \theta_T$, and \mathbf{v} is horizontal wind vector. After trial-and-error, a threshold of $\theta_T = 300.5$ K is used based on the θ boundary of the cold air mass (see Additional file 1: Fig. S3).

The cold pools developed at 17:00 LST have a DP thickness of ~ 60 hPa (Fig. 7a). At 20:00 LST, the initial cold pools spread over the basin, and new cold pools were generated due to new convective cells forming (Fig. 4j). Lifting of air along the leading edge of a cold pool has been known to trigger new convective cells (Fovell and Tan 1998; Rotunno et al. 1988; Tompkins 2001). The cold pool-driven convections in the basin are demonstrated by the low-level convergences in Fig. 7. Deep convection growth driven by cold pool interactions is found to be more effective when cold pool boundaries collide (Feng et al. 2015). In this case, the interaction

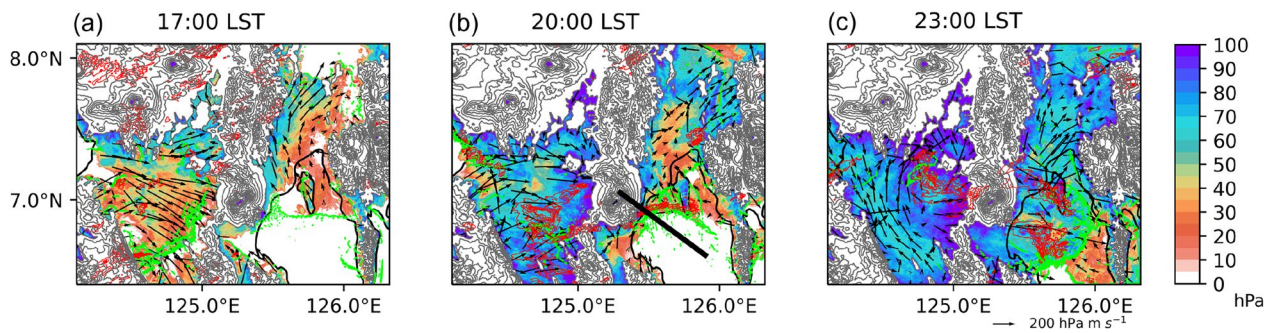


Fig. 7 Simulated DP (shade) and \vec{MF} (vectors) for $dx = 200$ m with topography (contour with intervals of 400 m), vertical velocity at 200 m height ($\geq 0.5 \text{ m s}^{-1}$; green contour, with an interval of 0.5 m s^{-1}), and rainfall (red contour, with an interval of 15 mm) at **a** 17:00 LST, **b** 20:00 LST, and **c** 23:00 LST. The black transect in **b** represents the cross-section used in Additional file 1: Fig. S5

of multiple cold pool outflow boundaries contributed to the upscale growth of convections to MCS-1 in the basin area. In addition, the cold air masses remained for hours in the basin (Fig. 7c), which suggests that the geometry of the concave basin also assisted in blocking the cold air masses within the basin area. The Froude numbers (Fr) are calculated to further support the topographic blocking around the basin (see Additional file 1: Fig. S4). Results show that Fr is always below 1 during the

duration of the case event, indicating that the airflow is blocked within the basin area.

Development of MCS-2 (east of Mount Apo)

MCS-2 developed separately over the Davao area, east of the Mount Apo terrain (refer to Fig. 4i). Southeasterly winds brought in low-level moisture from the ocean and interacted with the Mount Apo terrain resulting in convergence in the coastline (see Figs. 6d, 7b). The southeasterly winds at this time are due to the ambient trade

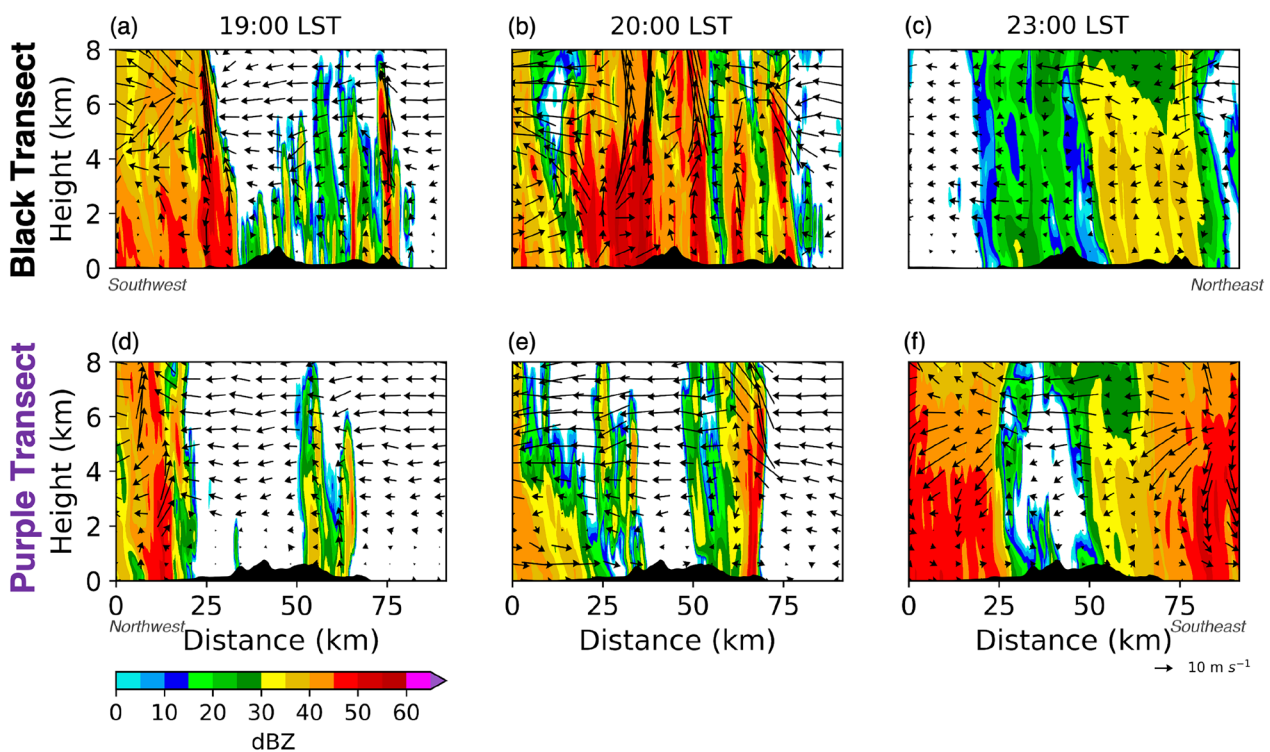


Fig. 8 Vertical structures of the simulated reflectivities of **a-c** black and **d-f** purple transects in Fig. 4i at 19:00 LST, 20:00 LST, and 23:00 LST for $dx = 200$ m. The black shades represent topography

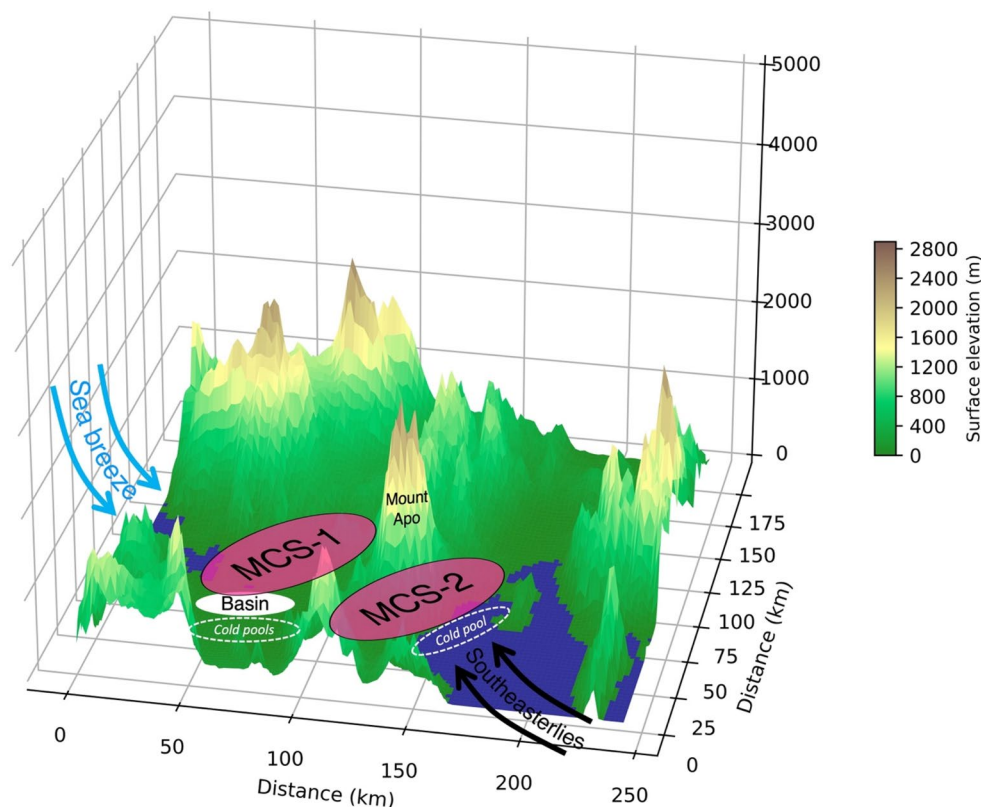


Fig. 9 Schematic diagram demonstrating the development of MCSs. Sea breeze on the western coast supplied the abundant moisture that developed MCS-1 in the basin. The precipitating downdrafts of MCS-1 formed cold pools that contributed to its upscale growth. The interaction of the southeasterly winds and Mount Apo terrain developed MCS-2, and its precipitating downdrafts formed a cold pool that assisted its maintenance and growth

winds. Rainfall developed over the southeast foot of Mount Apo at 20:00 LST (Fig. 7b) and a cold pool formed over the northeastern base of Mount Apo (Fig. 7b, c). A vertical cross-section of the cold pool is demonstrated by thermal buoyancy in Additional file 1: Fig. S5, where the initially developed cold air mass over the foot of the mountain expanded southeastward. As the cold air mass propagated southeastward, the cold air outflow strongly converged with the warm moist southeasterly flow. The continuous convergence between the cold air outflow and southeasterly flow resulted in the growth and maintenance of MCS-2 as new convective cells were initiated.

Merging and splitting of MCSs

As shown in the horizontal model reflectivity in Fig. 4i, j, MCS-1 and MCS-2 merged into a seemingly larger meso- β scale system (MCS-3) along the basin towards the Davao area at 20:00 LST. In reality, a river monitoring station (Matina Station of the DOST-ASTI) observed a peak water level of 4.73 m at 21:50 LST that resulted in the flooding of some areas in Davao City. The merging

of MCSs is further demonstrated in Fig. 8b, where the vertical cross-section of the black transect in Fig. 4i is shown. Considering that the merging process occurred during the evening, it is possible that the area growth and strength of the cold pools developing over time could have contributed to the merging of MCSs. Meanwhile, the splitting of MCS-3 to smaller meso- β scale MCSs occurred at 23:00 LST as the MCS over the Davao area propagated southeastward (Fig. 8f), and both MCSs subsequently weakened.

Summary and conclusion

During the summer season (April–May), MCS rainfall contributes a large fraction of the total rainfall over Mindanao Island, Philippines. This study examined the mechanisms involved in localized convection under weak large-scale forcing over Mindanao Island using high-resolution numerical simulations. A severe rainfall event on 03 May 2017 was chosen as the case study as it occurred during the summer season, where influences of large-scale systems (e.g., monsoonal flows, TCs) were

minimized. Results showed that the numerical simulations reasonably reproduced the heavy rainfall.

It is found that during the case event, two meso- β scale convective systems formed separately, west and east of Mount Apo terrain over Mindanao Island (referred to as MCS-1 and MCS2, respectively). MCS-1, located in the Mindanao basin area, formed mainly due to moisture advection from sea breeze circulation that resulted in the accumulation of moisture in the basin and made the area conducive for convection initiation. Cold pools were then generated from the precipitating downdrafts and the convergence of the outflow boundaries led to the upscale growth of MCS-1. Meanwhile, MCS-2, situated in the Davao area, formed as a result of interaction between southeasterly winds (ambient trade winds) and the high mountain terrain of Mount Apo. A cold pool was also generated from the precipitating downdrafts of MCS-2, where its outflow continuously converged with the southeasterly winds and maintained its development. At 20:00 LST, the two meso- β scale MCSs merged into a larger meso- β system (referred to as MCS-3). The long duration of rainfall accompanied by MCSs could have caused the flood over the Davao area. At 23:00 LST, MCS-3 began splitting with one of the MCSs moving southeastward. The processes involved in the development of the MCSs are visually summarized in the schematic diagram shown in Fig. 9.

This study gives insights into the importance of local processes (i.e., sea breeze circulation, cold air masses and terrain geometry) in the initiation and development of MCSs. In addition, the results demonstrated that the rainfall is more successfully captured in a sub-km scale resolution. These findings could be valuable in further understanding dynamics and improving weather forecasts of heavy rainfall associated with MCSs over the tropics.

Supplementary Information

The online version contains supplementary material available at <https://doi.org/10.1186/s40562-023-00277-8>.

Additional file 1. Table S1. Model configuration. Physics parameterizations are based on Tolentino and Bagtasa (2021). **Figure S1.** Seasonal percentage contribution of MCS rainfall to total rainfall for (a) DJF, (b) MAM, (c) JJA, and (d) SON over Mindanao Island, Philippines. The dataset used in the analysis is a subset of the recently developed global MCS database of Feng et al. (2021) covering 2000–2019. **Figure S2.** Hourly evolution of the vertical cross-section of wind speed (shade) with wind vectors, vertical velocity (pink contour, with an interval of 0.5 m s^{-1}), and cloud water mixing ratio (blue contour, with an interval of 0.5 g kg^{-1}) for $dx = 200 \text{ m}$. The cross-section is based on the black transect in Figure 6b. **Figure S3.** Hourly evolution of the vertical cross-section of potential temperature (white contour, with an interval of 0.5 K from 297 K to 300.5 K) over the basin cold pools for $dx = 200 \text{ m}$. The cross-section is based on the black transect in Figure 6b. **Figure S4.** (a) Hourly maximum Froude number (Fr) values of

$dx = 200 \text{ m}$ on the red box in (b); $Fr = U/NH$, where U is the average wind speed, N is Brunt–Väisälä frequency, and H is the mountain height. **Figure S5.** Hourly evolution of the vertical cross-section of thermal buoyancy (shade) with $\geq 1.0 \text{ m s}^{-1}$ vertical velocity (green contour, with an interval of 0.5 m s^{-1}), wind vectors, and topography (black shade) for $dx = 200 \text{ m}$. The cross-section is based on the black transect in Figure 7b.

Acknowledgements

This work is supported by the International Joint Graduate Program in Earth and Environmental Sciences, Tohoku University (GP-EES), JST SPRING Grant No. JPMJSP2114, JSPS KAKENHI Grant Nos. 19K03967 and 22H01295, and MEXT-Program for the Advanced Studies of Climate Change Projection (SENTAN) Grant No. JPMXD0722680734. This work used the supercomputing resources provided by the Cyberscience Center, Tohoku University. The authors gratefully acknowledge the Air Quality Dynamics and Instrumentation and Technology Development (AQD-ITD) Laboratory of Manila Observatory and DOST-ASTI, Philippines, for the observation measurements.

Author contributions

CL carried out the formal analysis, visualization, and writing—original draft. TY and JI provided supervision, funding, and writing—review and editing. All authors read and approved the final manuscript.

Funding

This research is funded by the International Joint Graduate Program in Earth and Environmental Sciences, Tohoku University (GP-EES), JST SPRING Grant No. JPMJSP2114, JSPS KAKENHI Grant Nos. 19K03967 and 22H01295, and MEXT-Program for the Advanced Studies of Climate Change Projection (SENTAN) Grant No. JPMXD0722680734.

Availability of data and materials

The datasets generated and/or analyzed in this study are available upon request from the corresponding author on reasonable request.

Declarations

Competing interests

The authors declare that they have no competing interests.

Received: 17 November 2022 Accepted: 24 April 2023

Published: 20 May 2023

References

- Bañares EN, Narisma G, Simpás JBB, Cruz FT, Lorenzo GRH, Cambaliza MOL, Coronel RC (2021) Seasonal and diurnal variations of observed convective rain events in Metro Manila, Philippines. *Atmos Res* 258:105646
- Du Y, Chen G, Han B, Bai L, Li M (2020) Convection initiation and growth at the coast of south China. Part II: effects of the terrain, coastline, and cold pools. *Mon Weather Rev* 148(2):3871–3892
- Du Y, Chen G, Han B, Mai C, Bai L, Li M (2020) Convection initiation and growth at the coast of south China. Part I: effect of the marine boundary layer jet. *Mon Weather Rev* 148(1):3847–3869
- Dudhia J (1989) Numerical study of convection observed during the winter monsoon experiment using a mesoscale two-dimensional model. *J Atmos Sci* 46(20):3077–3107
- Faustino-Eslava DV, Yumul GP Jr, Servando NT, Dimalanta CB (2011) The January 2009 anomalous precipitation associated with the “tail-end of the cold front” weather system in northern and eastern Mindanao (Philippines): natural hazards, impacts and risk reductions. *Global Planet Change* 76(1–2):85–94
- Feng Z, Hagos S, Rowe AK, Burleyson CD, Martini MN, de Szoeke SP (2015) Mechanisms of convective cloud organization by cold pools over tropical warm ocean during the AMIE/DYNAMO field campaign. *J Adv Model Earth Syst* 7(2):357–381

- Fovell RG, Tan P-H (1998) The temporal behavior of numerically simulated multicell-type storms. Part II: the convective cell life cycle and cell regeneration. *Mon Weather Rev* 126(3):551–577
- Hersbach H, Bell B, Berrisford P, Hirahara S, Horányi A, Muñoz-Sabater J, Nicolas J, Peubey C, Radu R, Schepers D et al (2020) The ERA5 global reanalysis. *Q J R Meteorol Soc* 146(730):1999–2049
- Hong S-Y, Lim J-OJ (2006) The WRF Single-Moment 6-class Microphysics scheme (WSM6). *Asia-Pac J Atmos Sci* 42(2):129–151
- Hsiao F, Chen Y-L, Hitzl DE (2020) Heavy rainfall events over central Oahu under weak wind conditions during seasonal transitions. *Mon Weather Rev* 148(10):4117–4141
- Iwasaki T, Shoji T, Kanno Y, Sawada M, Ujiiie M, Takaya K (2014) Isentropic analysis of polar cold airmass streams in the northern hemispheric winter. *J Atmos Sci* 71(6):2230–2243
- Kain JS (2004) The Kain–Fritsch convective parameterization: an update. *J Appl Meteorol* 43(1):170–181
- Kawashima M, Fujiyoshi Y, Ohi M, Mori S, Sakurai N, Abe Y, Harjupa W, Syamsudin F, Yamanaka MD (2011) Case study of an intense wind event associated with a mesoscale convective system in west Sumatera during the HARIMAU2006 campaign. *J Meteorol Soc Jpn Ser II* 89:239–257
- Keenan T, Rutledge S, Carbone R, Wilson J, Takahashi T, May P, Tapper N, Platt M, Hacker J, Sekelsky S et al (2000) The Maritime Continent—Thunderstorm Experiment (MCTEX): overview and some results. *Bull Am Meteor Soc* 81(10):2433–2456
- Kuo Y-H, Chen GT-J (1990) The Taiwan area mesoscale experiment (Tamex): an overview. *Bull Am Meteorol Soc* 71(4):488–503
- Macalalad RV, Xu S, Badilla RA, Paat SF, Tajones BC, Chen Y, Bagtasa G (2021) Flash flood modeling in the data-poor basin: a case study in Matina river basin. *Trop Cyclone Res Rev* 10(2):87–95
- Miao J-E, Yang M-J (2020) A modeling study of the severe afternoon thunderstorm event at Taipei on 14 June 2015: the roles of sea breeze, microphysics, and terrain. *J Meteorol Soc Jpn Ser II* 1:1
- Mlawer, E. J., Taubman, S. J., Brown, P. D., Iacono, M. J., & Clough, S. A. (1997). Radiative transfer for inhomogeneous atmospheres: RRTM, a validated correlated-k model for the longwave. *Journal of Geophysical Research: Atmospheres*, 102(D14), 16663–16682
- Mori S, Jun-Ichi H, Tauhid YI, Yamanaka MD, Okamoto N, Murata F, Sakurai N, Hashiguchi H, Sribimawati T (2004) Diurnal land-sea rainfall peak migration over Sumatera Island, Indonesian Maritime Continent, observed by TRMM satellite and intensive Rawinsonde soundings. *Mon Weather Rev* 132(8):2021–2039
- Natoli MB, Maloney ED (2019) Intraseasonal variability of the diurnal cycle of precipitation in the Philippines. *J Atmos Sci* 76(11):3633–3654
- Olaguera L, Matsumoto J, Dado J, Narisma G (2021) Non-tropical cyclone related winter heavy rainfall events over the Philippines: climatology and mechanisms. *Asia-Pac J Atmos Sci* 57(1):17–33
- Orlanski I (1975) A rational subdivision of scales for atmospheric processes. *Bull Am Meteorol Soc* 1975:527–530
- Pleim JE (2007) A combined local and nonlocal closure model for the atmospheric boundary layer. Part I: model description and testing. *J Appl Meteorol Climatol* 46(9):1383–1395
- Qian J-H (2008) Why precipitation is mostly concentrated over islands in the Maritime Continent. *J Atmos Sci* 65(4):1428–1441
- Rotunno R, Klemp JB, Weisman ML (1988) A theory for strong, long-lived squall lines. *J Atmos Sci* 45(3):463–485
- Schumacher RS, Rasmussen KL (2020) The formation, character and changing nature of mesoscale convective systems. *Nat Rev Earth Environ* 1(6):300–314
- Skamarock WC, Klemp JB, Dudhia J, Gill DO, Liu Z, Berner J, Wang W, Powers JG, Duda MG, Barker DM et al (2019) A description of the advanced research WRF model version, vol 4. National Center for Atmospheric Research, Boulder, p 145
- Tolentino JT, Bagtasa G (2021) Calibration of Kain–Fritsch cumulus scheme in Weather Research and Forecasting (WRF) model over western Luzon, Philippines. *Meteorol Atmos Phys* 133(3):771–780
- Tompkins AM (2001) Organization of tropical convection in low vertical wind shears: the role of cold pools. *J Atmos Sci* 58(13):1650–1672
- Wang S, Davies R, Gillies R (2013) Identification of extreme precipitation threat across midlatitude regions based on short-wave circulations. *J Geophys Res Atmos* 118(19):11–059
- Xiao X, Sun J, Ji L, Zhang L, Ying Z, Chen Z, Chen M, Xu C (2022) A study on local-scale thermal and dynamical mechanisms in the initiation of a squall line under weak forcing. *J Geophys Res Atmos* 127(5):e2021JD035561
- Yang G-Y, Slingo J (2001) The diurnal cycle in the tropics. *Mon Weather Rev* 129(4):784–801
- Yulihastin E, Hadi TW, Abdillah MR, Fauziah IR, Ningsih NS (2022) Propagation of convective systems associated with early morning precipitation and different northerly background winds over Western Java. *J Meteorol Soc Jpn Ser II* 1:1
- Yumul GP, Dimalanta CB, Servando NT, Cruz NA (2013) Abnormal weather events in 2009, increased precipitation and disastrous impacts in the Philippines. *Clim Change* 118(3):715–727
- Zhang Q-H, Lau K-H, Kuo Y-H, Chen S-J (2003) A numerical study of a mesoscale convective system over the Taiwan Strait. *Mon Weather Rev* 131(6):1150–1170

Publisher's Note

Springer Nature remains neutral with regard to jurisdictional claims in published maps and institutional affiliations.

Submit your manuscript to a SpringerOpen® journal and benefit from:

- Convenient online submission
- Rigorous peer review
- Open access: articles freely available online
- High visibility within the field
- Retaining the copyright to your article

Submit your next manuscript at ► [springeropen.com](https://www.springeropen.com)